



Human Hydroxyacid Oxidase (HAO1)



A Target Enabling Package (TEP)

| | |
|---------------------------------------|---|
| Gene ID / UniProt ID / EC | 54363 / Q9UJM8 / EC 1.1.3.15 |
| Target Nominator | Majid Fadhel (KAIMRC) |
| SGC Authors | Sabrina MacKinnon, Gustavo Arruda Bezerra, Tobias Krojer, Anthony R. Bradley, Romain Talon, Jose Brandao-Neto, Alice Douangamath, Udo Oppermann, Frank von Delft, Paul E. Brennan, Wyatt W. Yue |
| Collaborating Authors | N/A |
| Target PI | Wyatt W. Yue (SGC Oxford) |
| Therapeutic Area(s) | Metabolic disorders |
| Disease Relevance | In peroxisomal glyoxylate metabolism, HAO1 is the enzyme upstream of AGXT, mutations of which cause Primary Hyperoxaluria type 1 (OMIM 259900) |
| Date Approved by TEP Evaluation Group | 13 th June 2018 |
| Document version | Version 2 |
| Document version date | April 2019 |
| Citation | Sabrina MacKinnon, Gustavo Arruda Bezerra, Tobias Krojer, Anthony R. Bradley, Romain Talon, Jose Brandao-Neto, ... Wyatt W. Yue. (2018). Human Hydroxyacid Oxidase (HAO1); A Target Enabling Package. Zenodo. http://doi.org/10.5281/zenodo.1342617 . |
| Affiliations | N/A |

We respectfully request that this document is cited using the DOI reference as given above if the content is used in your work.

USEFUL LINKS



Open Targets



IMPC
International Mouse Phenotyping Consortium

ChEMBL



(Please note that the inclusion of links to external sites should not be taken as an endorsement of that site by the SGC in any way)

SUMMARY OF PROJECT

This project provides the tools and data to develop small molecule inhibitors for an inherited metabolic disorder (Primary hyperoxaluria type 1) due to the defective enzyme (AGXT), by targeting the enzyme (HAO1) upstream of the glyoxylate metabolic pathway to mitigate the defect (i.e. substrate reduction approach). This TEP package includes recombinant human HAO1 purification protocols, structures of the HAO1 in different states, *in vitro* assays to detect ligand/inhibitor binding (DSF, SPR) and enzyme activity (amplex red assay) of human HAO1, as well as initial chemical matters identified from crystallography-based fragment screening.

SCIENTIFIC BACKGROUND

Genetic linkage

Glyoxylate is a highly reactive molecule generated through the oxidation of glycolate in peroxisomes and the catabolism of hydroxyproline in mitochondria. These pathways represent the end-product of the metabolism of several amino acids (e.g. glycine) and sugars (e.g. glucose, fructose). Under normal conditions, glyoxylate is rapidly detoxified into glycine through the peroxisomal enzyme alanine-glyoxylate aminotransferase (AGXT, EC 2.6.1.44). Primary hyperoxaluria type 1 (PH1) is an autosomal recessive disorder caused by loss-of-function mutations in the AGXT gene (OMIM 259900) (Fig 1, red) (1). The principal hallmark of PH1 is deposition of insoluble calcium oxalate stones from the oxidation of glyoxylate, which accumulates due to deficient AGXT activity in hepatocyte peroxisomes. The main target organ for accumulation of calcium oxalate stones is the kidney, commonly leading to end stage renal disease. As kidney function declines, calcium oxalate is also deposited in other tissues e.g. heart, nerves, bone, eyes and bone marrow (2).

Unmet need

To date there is no transformative therapy for PH1 (3). For a subset (~30%) of PH1 patients, the disease process is slowed down by supplementation of pyridoxine, the precursor for the AGXT enzyme cofactor pyridoxal 5'-phosphate. For pyridoxine non-responsive patients, the only treatment option is combined liver and kidney transplant with risk of morbidity and immunosuppression. PH1 is a poor target for gene and enzyme replacement therapies, as curative treatment requires correction of oxalate overproduction in the majority of hepatocytes and these methods are not currently capable of high enough efficiency.

Rationale

We propose that the substrate reduction approach to inhibit the biosynthesis of glyoxylate, the precursor of oxalate, could provide therapeutic benefit for PH1 by reducing the pool of glyoxylate available for oxidation to insoluble oxalate. One target enzyme for inhibition is glycolate oxidase (also known as hydroxyacid oxidase, HAO1) (Fig 1, blue)(4) which catalyses the conversion of glycolate to glyoxylate and to a lesser extent the subsequent oxidation to oxalate.

- In the pathway of glyoxylate production, HAO1 is the enzyme immediately upstream of AGXT, the causative defect for PH1. HAO1 is primarily expressed in liver and pancreas (4).
- Individuals carrying rare HAO1 mutations are reported as asymptomatic (5).
- siRNA targeting HAO1 reduced urinary oxalate by 50% in a PH1 mouse model (AGXT^{-/-}) (6,7), with similar results in disease model from other primates (8).

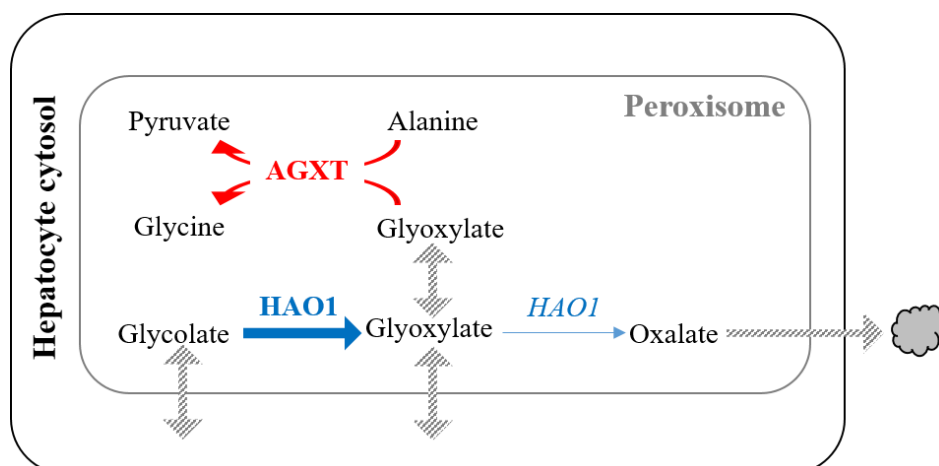


Figure 1 Pathway of glyoxylate production in liver peroxisome

Proteins Purified

Human HAO1

HAO1 catalyses the FMN-dependent oxidation of glycolate to glyoxylate. It belongs to the class of 2-hydroxyacid oxidases involved in the peroxisomal oxidation of 2-hydroxyacid intermediates generated in the alpha oxidation pathway to hydrogen peroxide (H₂O₂) and keto-acids. We have generated the full-length construct (aa 1-370) as well as a nested set of constructs with varying N-terminal (Met1, Leu5, Ile8) and C-terminal (Pro364, Ser368, Ile370) boundaries for human HAO1 (hHAO1), all yielding high levels of soluble recombinant protein when expressed in *E. coli*.

Structural data

hHAO1 structures

We have determined two high resolution (1.35 Å) crystal structures of hHAO1 bound with FMN (**Fig 2A**). One structure (PDB 2NZL) captures the product glyoxylate at the active site, and the other structure is bound with the substrate glycolate (PDB 6GMB). Our structural data reveal substrate-induced ordering of the loop 4 (aa 169-212) between strand β₄ and helix α₄, which guards access to the active site. Loop 4 is disordered in the product-bound structure, and adopts varying conformations in the fragment-bound structures as described in latter sections.

The hHAO1 structure displays an 8-stranded α/β TIM barrel motif typical for the family of L-2-hydroxyacid oxidases and dehydrogenases (**Fig 2A**). The active site of hHAO1 is located at the loops (e.g. loop 4) found at the C-terminal end of the barrel β-strands. The FMN cofactor is located in a hydrophobic pocket and held in place by multiple polar interactions. Our structures reveal subtle differences in the configuration between the glycolate substrate (non-planar) and product glyoxylate (planar), with glycolate in a position poised for its proton to be abstracted on its way to form the carbanion intermediate (**Fig 2B**).

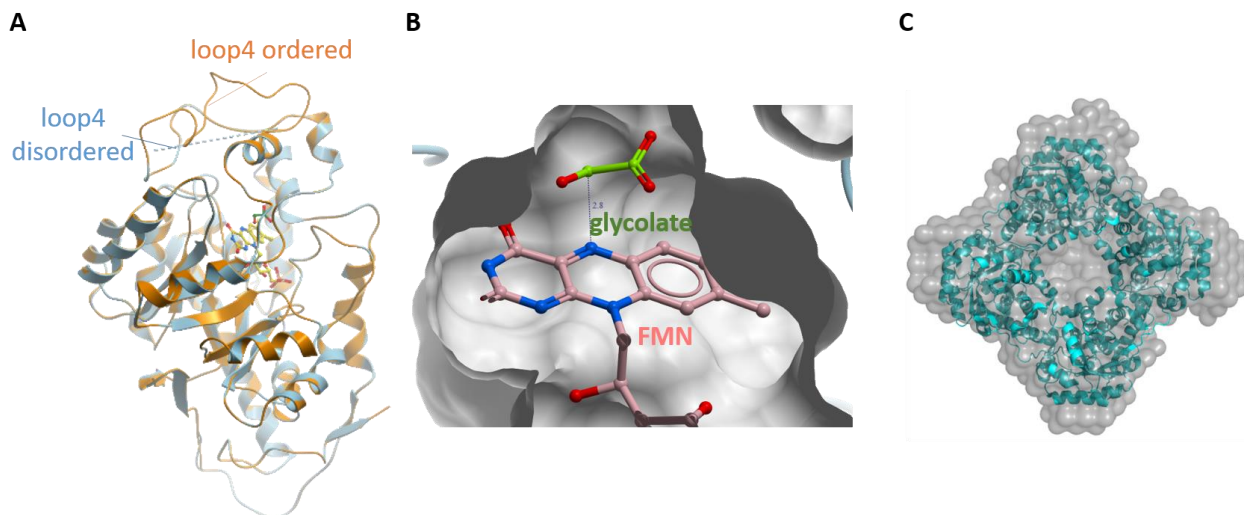


Figure 2 (A) Structure of hHAO1 protomer revealed by the substrate-bound (orange) and product-bound (blue) structures. (B) Surface representation of the active site bound with glycolate and FMN, showing the distance between glycolate α-carbon and FMN N5 nitrogen favourable for hydride transfer. (C) *Ab initio* SAXS model of hHAO1 tetramer overlaid with crystal structure.

The hHAO1 protomer in the crystal asymmetric unit forms homo-tetramers with neighbouring subunits in the unit cell, resulting in C4 symmetry. The primary monomer-monomer interface is formed by the loop connecting the first two β -strands β 1- β 2 (aa 51-60) and the last helix α 8 (aa 335-350) from one monomer, and helix α D within loop 4 (aa 163-171) from the other monomer. The hHAO1 tetramer is confirmed in solution by size exclusion chromatography (SEC), as well as by small angle x-ray scattering (SAXS)(Fig 2C).

In vitro assays

Differential scanning fluorimetry

We applied the thermal shift assay (differential scanning fluorimetry) to detect binding of native ligands of hHAO1 by ligand-induced thermal stabilization. The enzyme cofactor FMN (0.1 mM) causes a shift in melting temperature (ΔT_m) of 10.8 °C to the as-purified protein (2 μ M), while the substrate glycolate (5 mM) causes a ΔT_m of 6.5 °C.

Fluorescence activity assay

We followed H_2O_2 formation during hHAO1-catalysed oxidation of glycolate to glyoxylate by coupling the reaction with horseradish peroxidase and a reporter substrate, Amplex Red. In the presence of H_2O_2 , horseradish peroxidase oxidises Amplex Red to fluorescent resorufin, allowing fluorescence emission detection at 590 nm (Fig 3A). Using this assay, the *in vitro* activity of purified hHAO1 obeys Michaelis-Menten kinetics, displaying a clear substrate preference for the short chain 2-hydroxyacid glycolate (Fig 3B blue, K_M of 18.5 μ M), as opposed to long-chain 2-hydroxyacids (e.g. 2-hydroxypalmitate, Fig 3B green) with 100-fold higher K_M for the latter.

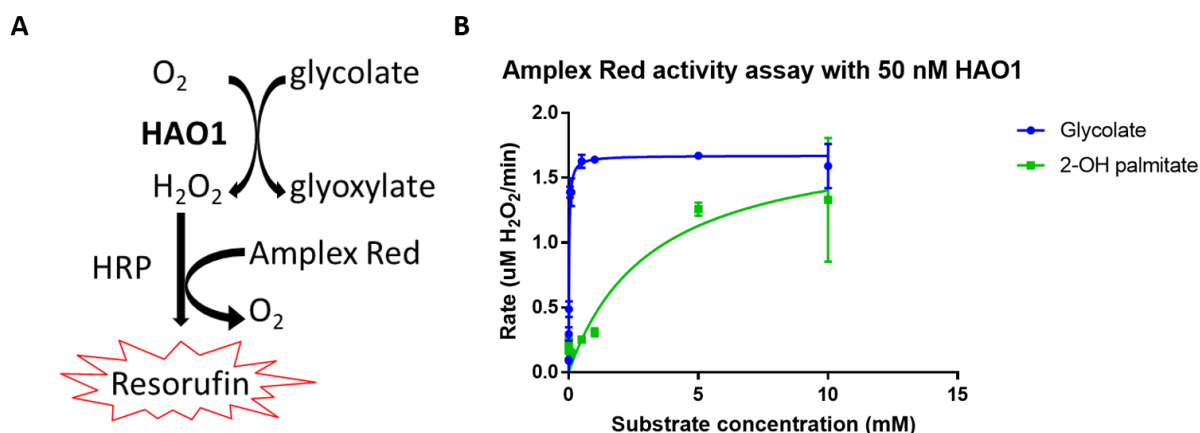


Figure 3 In vitro activity assay of hHAO1 (A) employing the Amplex red reagent that couples H_2O_2 product formation with fluorescence detection, (B) determining the substrate preference for the short-chain glycolate.

Chemical Matters

Crystallography-based fragment screening

Given that the series of hHAO1 full-length and truncation constructs all yielded soluble proteins, we first interrogated their ability to reproduce diffracting crystals with the quality and consistency appropriate for a medium throughput fragment screening campaign. To facilitate this, we applied an in-house experimental procedure known as 'PREPX' (9) that processes dozens of constructs from expression through purification and crystallization within a week. We found that hHAO1₁₋₃₆₈ yields the most reproducible crystals with best diffraction quality. We first demonstrated the 'soak-ability' of our crystal form by determining the 1.2 Å structure of hHAO1 in complex with a tool compound for the class of 2-hydroxyacid oxidases, 4-carboxy-5-[(4-chlorophenyl)sulfonyl]-1,2,3-thiadiazole (CCPST, PDB 6GMC), extending previously reported data at 2.8 Å resolution (PDB 2WOU).

A crystallography-based fragment screening campaign ('XChem')(9) was then carried out using hHAO1₁₋₃₆₈. In total, data sets for 409 hHAO1 crystals, each soaked with an individual fragment, have been collected and processed. This campaign yielded 17 bound fragments, 7 of which are clustered in three functionally relevant regions of the hHAO1 structure (PDB codes 5QIB-H) (**Fig 4**). An overview of bound fragments to HAO1 can be found in **Figure 9**.

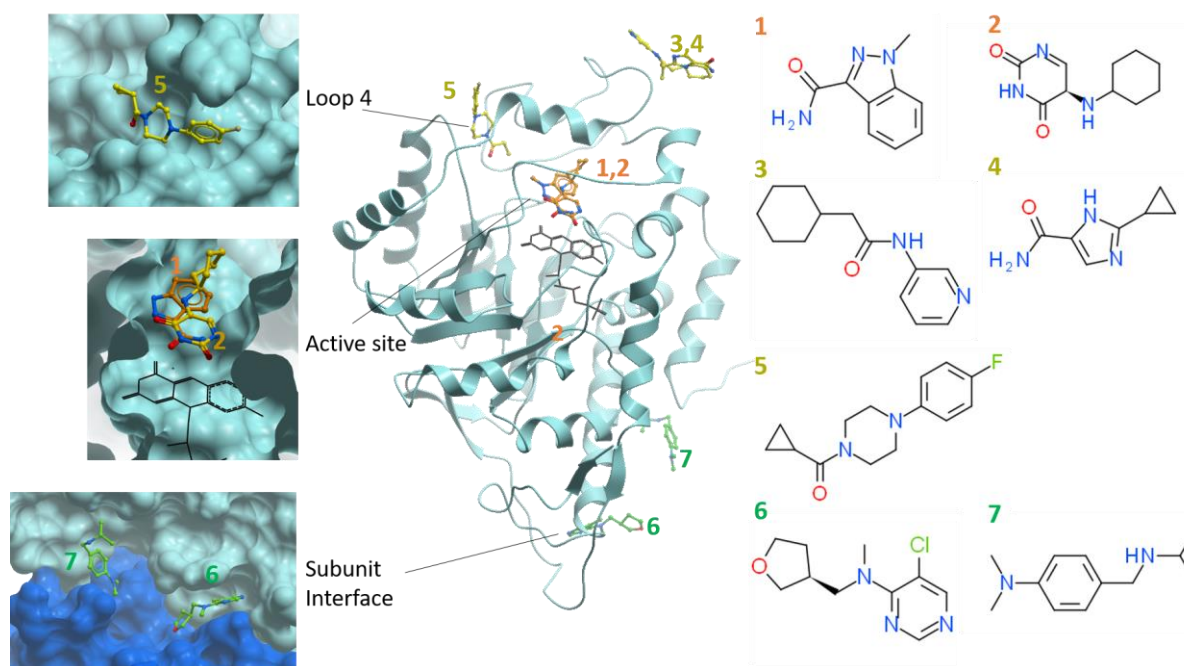


Figure 4 hHAO1-bound fragments clustered in 3 functionally relevant regions of the protein

The identified functional sites are as follows:

- (1) Two fragments (**1,2**) were identified at the **active site**, overlaying where the substrate glycolate binds adjacent to FMN (**Fig 5**). These fragments engage directly with residues involved in native ligand binding and catalysis. The active site displays a large degree of plasticity in accommodating these fragments. We identified 3 loop regions (aa 109-110, 164-175, 205-209) that undergo concerted main-chain displacement in the fragment-bound structures (**Fig 5, orange & cyan lines**), compared with the substrate-bound 'ground state' (**Fig 5, grey lines**). The largest displacement is within the helical segment αE of loop 4 (aa 204-212), with $C\alpha$ changes of 2-4 Å for Leu205, Ala206 and Val209. There are also changes in side-chain conformations for Tyr26, Met82, Trp110, His260 and Arg263. Importantly, to accommodate the fragments, the bulky Trp110 indole ring either swings away by $\sim 180^\circ$ from the active site to avoid steric clash (fragment **2**), or in the case of fragment **1** the entire Trp110-containing loop region is displaced from the active site by 4.5 Å. Residue Trp110 enables the enzyme to fit and operate on the short-chain substrate glycolate, while binding of larger fragments/inhibitors can also be mediated by the conformational flexibility of the Trp110 side-chain to make room in the active site.

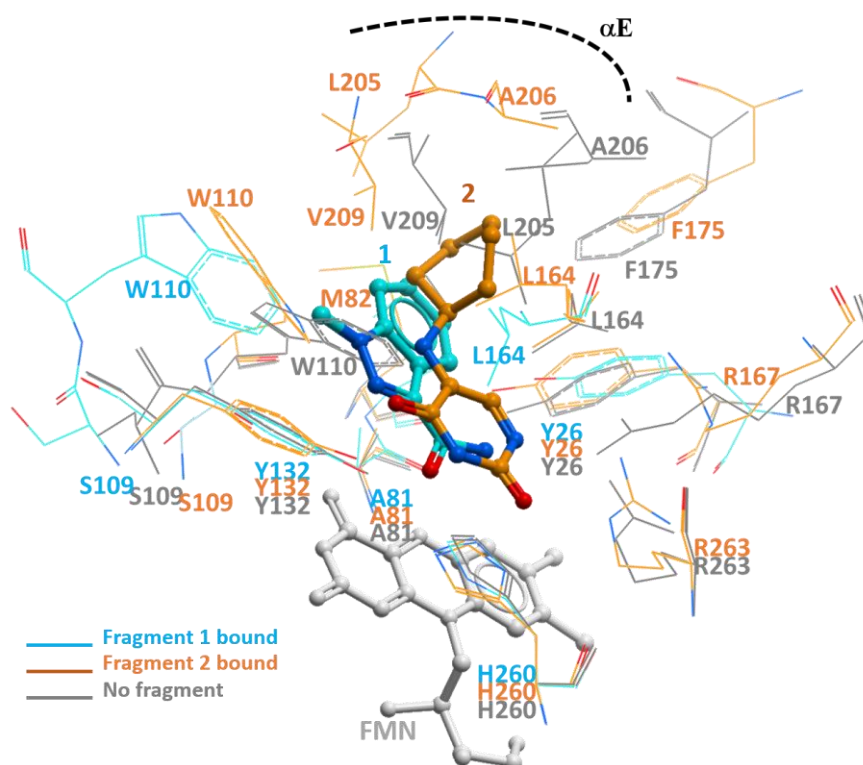


Figure 5 Binding mode for fragments 1 (cyan) and 2 (orange) in the active site. Amino acids in the binding site that show conformational changes in the fragment-bound structures (colour-coded by fragment), compared to the substrate-bound state (grey), are shown. Cofactor FMN is also shown as sticks.

(2) Three fragments are observed in proximity to the **loop 4 region**, close to the protein surface. Two (**3,4**) are clustered in a region where interactions are partly mediated by neighbouring symmetry-related subunit (not shown). The other fragment (**5**) (**Fig 6**) is bound in a hydrophobic pocket at loop 4, close to the active site but separated from the two active site fragments (**1,2**) by the helical segment αE . Compared to the ground state structure (**Fig 6, violet vs grey lines**), binding of fragment 5 near loop 4 also shifts the orientation of helix αE to bring Tyr208, Val209 and Ala212 into interacting with the fragment, as well as displaces the bulky Trp110 side-chain.

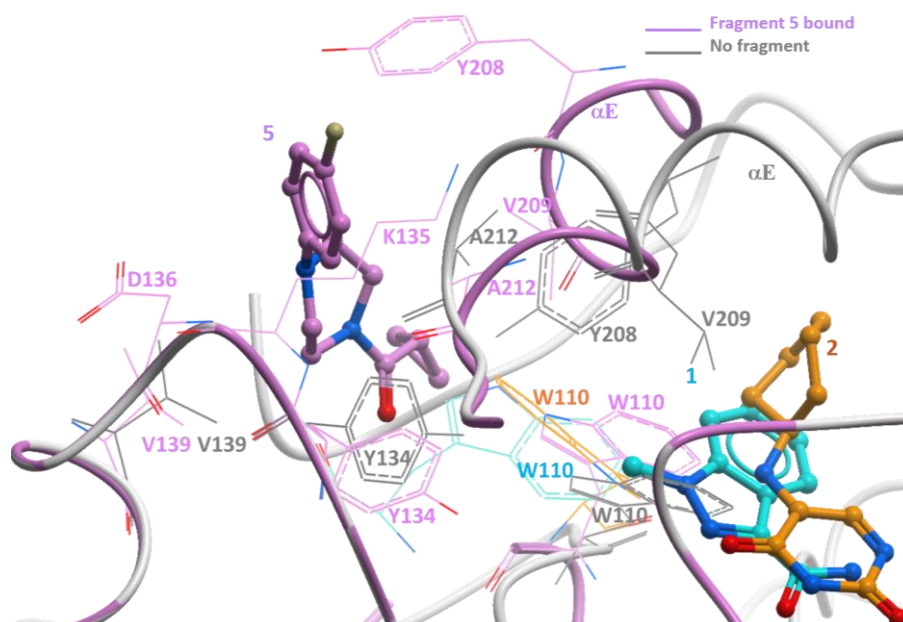


Figure 6 Binding mode for fragment 5 in proximity to the loop 4 region. Amino acids in the binding site that show conformational changes in the fragment-bound structure (violet), compared to the substrate-bound state (grey), are shown. Binding locations for fragments 1 and 2 in the active site are also shown for reference.

(3) The final two fragments occupy the primary **monomer-monomer interface** of the hHAO1 tetramer (**6,7**). These fragments are bound in a hydrophobic pocket formed by the N-terminal (Ile6 of loop β 1- β 2) and C-terminal (Ile335 and Leu342 of helix α 8) ends of one subunit, as well as the less mobile region in loop 4 (Tyr163 and Val171 of helix α D) of the adjacent subunit of the homo-tetramer (**Fig 7**). Binding of fragment **6** is further enhanced by π - π aromatic stacking between the fragment's pyrimidine ring and side-chain of Tyr163.

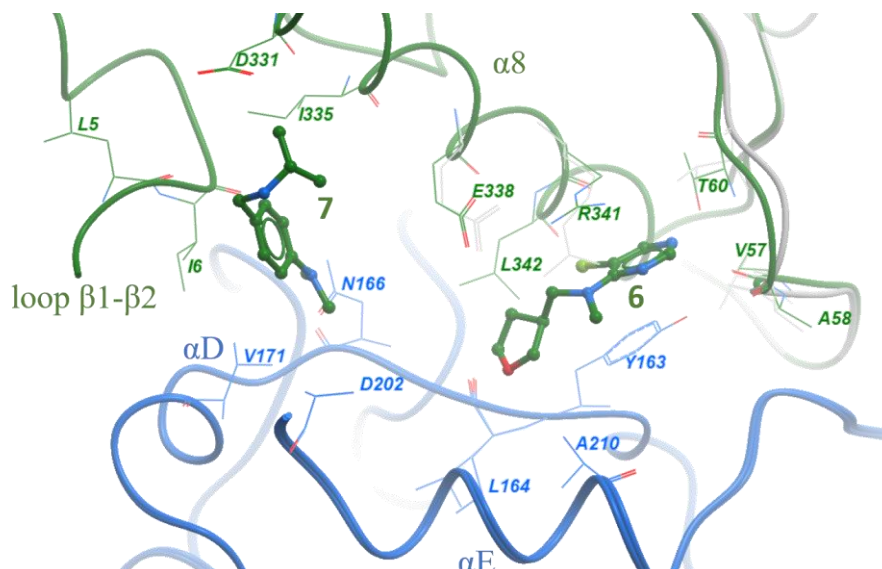


Figure 7 Binding mode for fragments **6** (right) and **7** (left) at the monomer-monomer interface. Amino acids that interact with the fragments are shown, coloured green for one subunit, and blue for the other subunit of the interface.

We next selected four of the bound fragments hits (**Fig 8A**; **1, 2, 5, 6**), on the basis of their extensive interaction with the protein, for further biophysical characterization using *in vitro* activity assay and surface plasmon resonance (SPR). SPR demonstrated weak binding for all four fragments to hHAO1 at high μ M concentration range (**Fig 8B**). In the activity assay (**Fig 8C**), hHAO1 enzyme is inhibited by the active site fragment **1** (IC_{50} of 420 μ M, $LE = 0.36$), to a lesser extent by the active site fragment **2** and the loop fragment **5**, but not inhibited by fragment **6** at the interface as expected from its binding location.

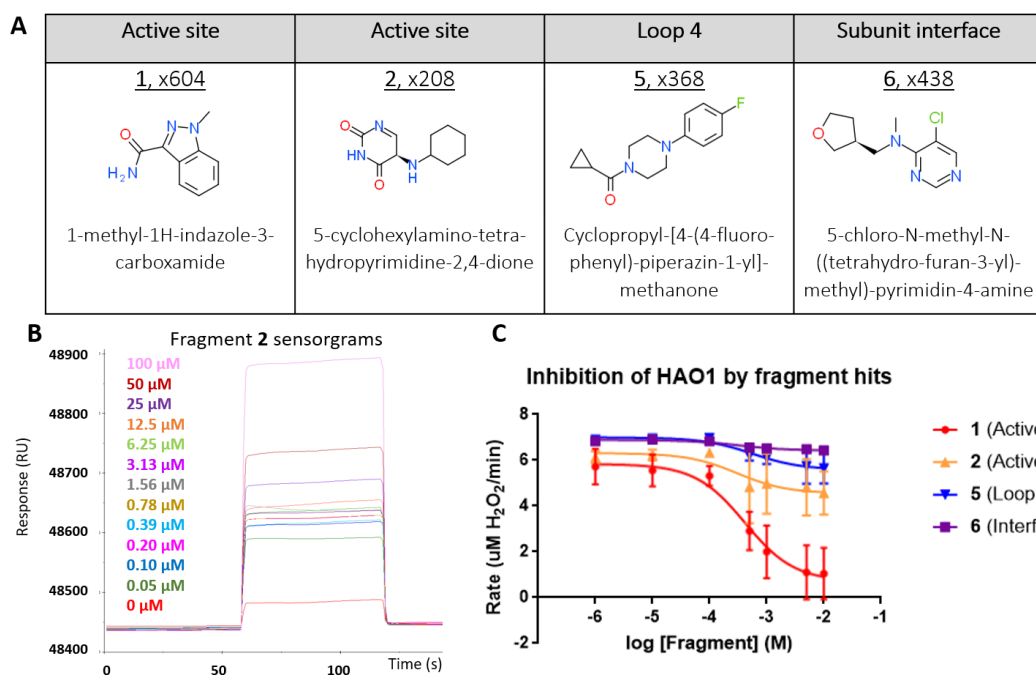


Figure 8 (A) Table of fragments selected for follow-up characterization, showing crystal ID, chemical structure and IUPAC name for each fragment. (B) Example sensorgram for the binding of active site fragment **2** to immobilized His-hHAO1. (C) Determination of enzyme inhibition by the four fragments using the fluorescence activity assay.

Overview of Bound Fragments to HAO1

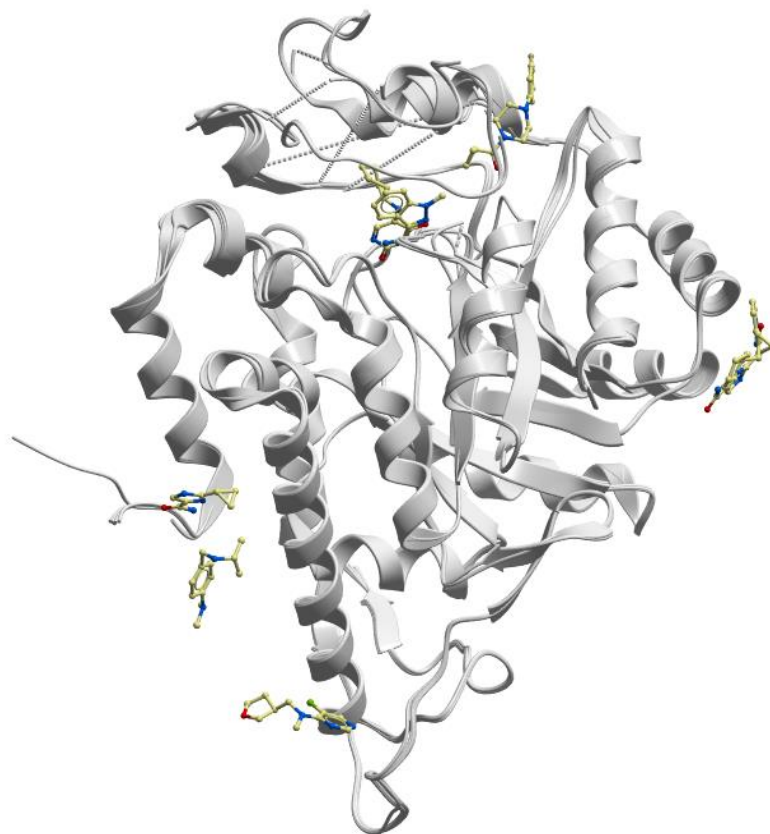
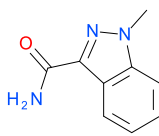
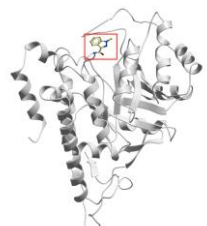
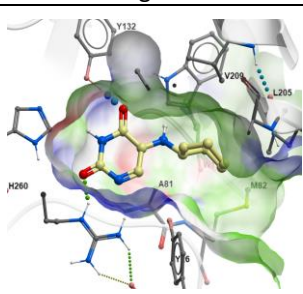
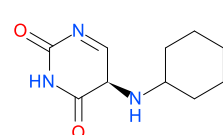
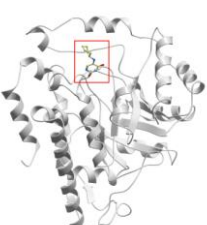
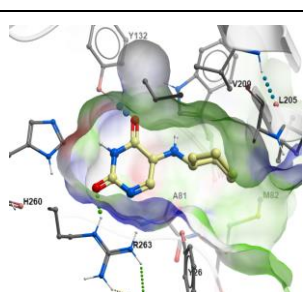
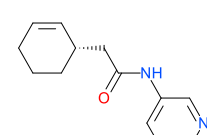

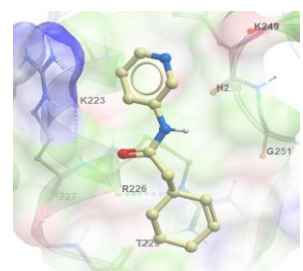
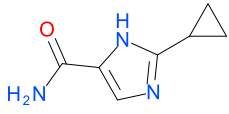
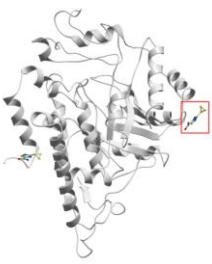
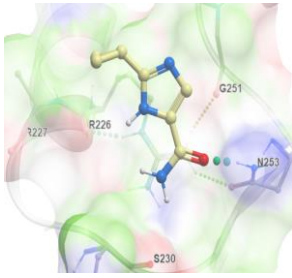
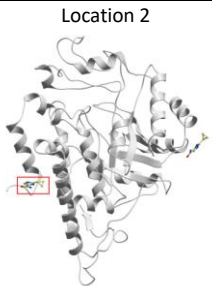
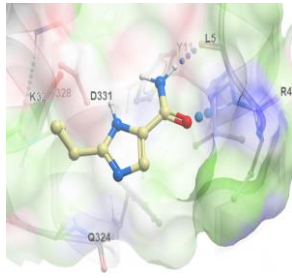
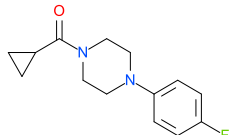
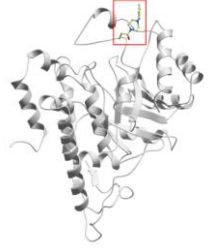
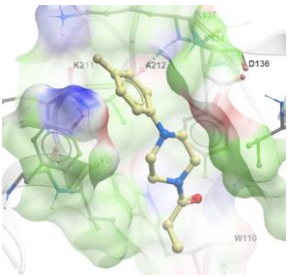
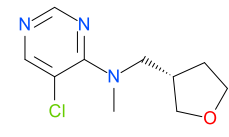

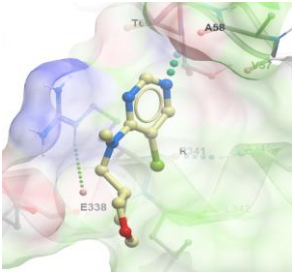
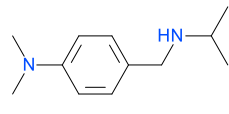
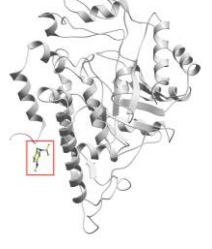
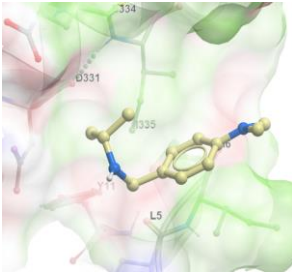


Figure 9 Overview of HAO1 layered with bound ligands.

| PDBID | Ligand | Binding Location | Binding Pocket | Resolution (Å) |
|------------------|--|---|--|----------------|
| 5QIH 1 |  FM010692a |  |  | 1.33 |
| 5QIB 2 |  FM010068a |  |  | 1.48 |
| 5QIF 3 |  FM001935b |  |  | 1.2 |

| | | | | |
|-----------|--|---|--|------|
| 5QIG 4 |  FM010691a | Location 1  |  | 1.42 |
| | | Location 2  |  | |
| 5QIC 5 |  FM010032b |  |  | 1.34 |
| 5QID 6 |  FM010689a |  |  | 1.45 |
| 5QIE 7 |  FM010690a |  |  | 1.34 |

IMPORTANT: Please note that the existence of small molecules within this TEP only indicates that chemical matter can bind to the protein in a functionally relevant pocket. As such, these molecules should not be used as tools for functional studies of the protein unless otherwise stated as they are not sufficiently potent or well-characterised to be used in cellular studies. The small molecule ligands are intended to be used as the basis for future chemistry optimisation to increase potency and selectivity and yield a chemical probe or lead series.

CONCLUSION

Summary

The structural and chemical biology data from this TEP project have provided a path for inhibitor development of hHAO1, as substrate reduction therapy for the metabolic disorder PH1. Our high resolution structures have revealed the binding modes for the native substrate, product and cofactor, and the ligand-

induced conformational changes in an extensive loop 4 segment. Crystallography-based fragment screening have yielded chemical starting points at 3 functionally relevant sites, which have been validated and further characterized by our activity and binding assays. The active site and the neighbouring loop residues of hHAO1 demonstrate clear conformational plasticity in accommodating different binding modes of fragments, providing ample opportunities to be exploited for structure-based drug design.

Ongoing and Future work

Enabled by the recently awarded add-on grant from the Wellcome TEP project, > 200 follow-up compounds have been acquired commercially as the next step of fragment optimisation, based on the chemical scaffolds from the four fragments characterized in this work. These follow-up compounds were characterised by our in vitro activity assay resulting in improved hits (IC₅₀ < 100 μM) from each of the four fragments: compound **8** based on fragment **1** (IC₅₀ 62 μM); compound **9** from fragment **2** (IC₅₀ 65 μM); compounds **10**, **11** and **12** from fragment **5** (IC₅₀s 45, 58 and 69 μM respectively); and compound **13** from fragment **6** (IC₅₀ 86 μM). Co-crystallisation and crystal soaking experiments are currently ongoing, alongside SPR experiments, to characterise the binding of these compounds.

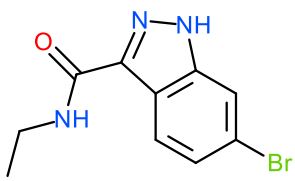
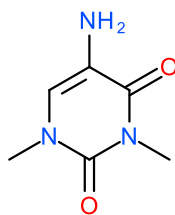
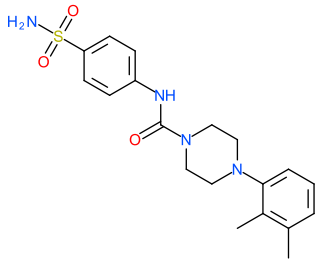
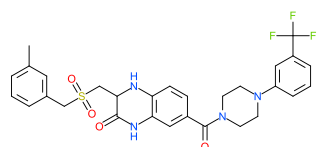
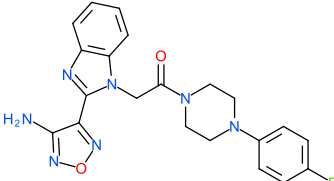
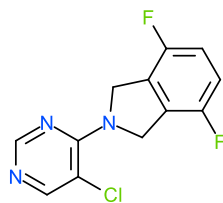
| 8, from active site fragment 1 | 9, from active site fragment 2 | 10, from loop fragment 5 |
|--|---|--|
|  <p data-bbox="175 1097 566 1176">6-bromo-N-ethyl-1H-indazole-3-carboxamide</p> |  <p data-bbox="614 1097 981 1176">5-amino-1,3-dimethylpyrimidine-2,4-dione</p> |  <p data-bbox="1037 1086 1412 1187">4-(2,3-dimethylphenyl)-N-(4-sulfamoylphenyl)piperazine-1-carboxamide</p> |
| 11, from loop fragment 5 | 12, from loop fragment 5 | 13, from interface fragment 6 |
|  <p data-bbox="175 1556 566 1724">3-[(3-methylphenyl)methylsulfonylmethyl]-7-[4-[3-(trifluoromethyl)phenyl]piperazine-1-carbonyl]-3,4-dihydro-1H-quinoxalin-2-one</p> |  <p data-bbox="598 1568 989 1713">2-[2-(4-amino-1,2,5-oxadiazol-3-yl)benzimidazol-1-yl]-1-[4-(4-fluorophenyl)piperazin-1-yl]ethanone</p> |  <p data-bbox="1037 1568 1412 1713">8-(5-chloro-pyrimidin-4-yl)-2,5-difluoro-8-aza-bicyclo[4.3.0]nona-1(6),2,4-triene</p> |

Figure 10 Overview of improved potency follow-up compounds based on fragments 1, 2, 5 and 6.

There is recent evidence from siRNA knock-down (6) that inhibition of other enzymes that contribute to glyoxylate production, such as human hydroxyproline dehydrogenase (hPRODH2) which converts hydroxyproline to pyrroline-5-carboxylate in the mitochondria (10), may also be considered a therapeutic target by the substrate reduction approach. We have yielded soluble expression constructs of hPRODH2, and have scaled up for crystallization trial.

We have recently submitted a grant application to the Oxalosis & Hyperoxaluria Foundation, with a proposal to support chemistry optimization of hHAO1 fragments and structural biology of hPRODH2. Our proposal has received favourable reviews and we have been invited to submit a revision for the next funding round. Collaborations have also been established to test and validate lead compounds arising from this project in patient-derived cells/organism model (Ronald Wanders, Amsterdam; Majid Fadhel, KAIMRC).

FUNDING INFORMATION

The work performed at the SGC has been funded by a grant from the Wellcome [106169/ZZ14/Z].

ADDITIONAL INFORMATION

Structure Files

| PDB ID | Structure Details | Supplier |
|----------------------|--|--|
| 2NZL | hHAO1-FMN, bound with glyoxylate, disordered loop 4 | |
| 6GMB | hHAO1-FMN, bound with glycolate, ordered loop 4 | |
| 6GMC | hHAO1-FMN, bound with CCPST inhibitor | |
| 5QIB | hHAO1-FMN, bound with fragment 2 (crystal x208) | Crea-Chim UAB |
| 5QIC | hHAO1-FMN, bound with fragment 5 (crystal x368) | Diamond Light Source XChem facility |
| 5QID | hHAO1-FMN, bound with fragment 6 (crystal x438) | Diamond Light Source XChem facility |
| 5QIE | hHAO1-FMN, bound with fragment 7 (crystal x518) | Diamond Light Source XChem facility |
| 5QIF | hHAO1-FMN, bound with fragment 3 (crystal x566) | Diamond Light Source XChem facility |
| 5QIG | hHAO1-FMN, bound with fragment 4 (crystal x603) | Diamond Light Source XChem facility |
| 5QIH | hHAO1-FMN, bound with fragment 1 (crystal x604) | Diamond Light Source XChem facility |

Non-SGC resources

| Commercially available CRISPR/Cas9 knockout plasmids |
|---|
| SCBT: Cat # sc-407493 |
| Genscript: Cat # 54363 These sgRNA sequences were validated in Sanjana N.E., Shalem O., Zhang F. Improved vectors and genome-wide libraries for CRISPR screening . Nat Methods. 2014, 11(8):783-4. |
| Commercially available antibodies |
| Thermofisher: MA5-24346 (monoclonal) |
| SCBT: sc-517552 (monoclonal) |

Materials and Methods

Protein expression and purification of hHAO1

Vector: pNIC28-Bsa4

Entry Clone Accession: NM_017545

Cell line: BL21 (DE3)-R3/Rosetta

Tags and additions: N-terminal, TEV protease cleavable hexahistidine tag

Construct protein sequence:

Mhhhhhssgvdltgenlyfq*sMLPRLICINDYEQHAKSVLPKSIYDYRSGANDEETLADNIAAFSRWKLY
PRMLRNVAETDLSTSVLQQRVSMPICVGATAMQRMHVVDGELATVRACQSLGTGMMLSSWATSSIEEVAEAGP
EALRWLQLYIYKDREVTKKLVQRQAEMGYKAI FVTVDTPYLG NR LDDVRNRFKLPPQLRMKNFETSTLSFSPE
ENFGDSSGLAAYVAKAIDPDISWEDIKWLRLTSLPIVAKGILRGDDAREAVKHGLNGLVSNHGARQLDGVP
ATIDVLP EIVEAVEGKVEVFLDGGVVRKGT DVLKALALGAKAVFVGRPIVWGLAFQGEKGVQDVLEILKEEFRL
AMALSGCQNVKVIDKTLVRKNPLAVSKI

(Underlined sequence contains vector encoded His-tag and TEV protease cleavage site*)

An overnight culture (20 mL LB) was used to inoculate 2L auto-induction TB containing 50 µg/ml each of kanamycin and chloramphenicol. Cells were cultured at 37°C for 6 hours followed by 48 h incubation at 18°C.

Extraction Buffer: 500 mM NaCl, 50 mM HEPES pH 7.5, 20 mM imidazole, 0.5 mM TCEP, 5% glycerol, 1:1000 of Merck Protease Cocktail II, 0.5 mg/mL lysozyme and 0.2 µg/mL benzonase.

Binding Buffer: 500 mM NaCl, 50 mM HEPES pH 7.5, 20 mM imidazole, 0.5 mM TCEP, 5% glycerol.

Washing Buffer: 500 mM NaCl, 50 mM HEPES pH 7.5, 40 mM imidazole, 0.5 mM TCEP, 5% glycerol.

Elution Buffer: 500 mM NaCl, 50 mM HEPES pH 7.5, 250 mM imidazole, 0.5 mM TCEP, 5% glycerol.

GF buffer: 500 mM NaCl, 50 mM HEPES pH 7.5, 0.5 mM TCEP, 5% glycerol.

Cell pellet from 2 L of culture was re-suspended in 150 mL Extraction Buffer, lysed by sonication for 15 minutes, and centrifuged at 37000 x g for 1 hour at 4°C. The clarified cell extract was incubated with 5 mL of Ni-NTA resin pre-equilibrated with lysis buffer before applying to 1.5 x 10 cm column by gravity flow. The column was washed with 10 column volumes of Binding Buffer, 10 column volumes of Wash Buffer, and eluted with 5 x 5 mL Elution Buffer. Fractions containing hHAO1 were loaded onto gel filtration column (Superdex 200 Hiload 16/60) pre-equilibrated with GF buffer. Fractions containing hHAO1 were pooled.

Activity assay

The catalytic activity of hHAO1 was measured by the Amplex Red assay. We adopted the assay in 96 well format for detection using the PheraStar FSX fluorescence reader (BMG Labtech)(Excitation/Emission = 560/590 nm). Michaelis-Menten kinetics were determined by incubating 100 nM protein with substrate (0.5 µM - 10 mM) at room temperature for 10 minutes, adding Amplex Red reagent (0.01U horseradish peroxidase and 50 µM Amplex Red), incubating for a further 10 minutes, and measuring the resultant fluorescence. The reaction buffer consists of 50 mM sodium phosphate, pH 7.4, 200 mM KCl, 2 mM MgCl₂ and 0.01% TritonX. This assay gave a linear response with protein concentration up to 200 nM and H₂O₂ production up to 50 µM. Standard curve ranging from 0 – 50 µM H₂O₂ was used to calculate reaction rate (µM H₂O₂ / min). To test fragments for their effect on hHAO1 activity, protein was pre-incubated with fragment compound (0.1 µM - 10 mM) for 10 minutes before addition of substrate (720 µM glycolate) and following procedures above.

Differential scanning fluorimetry

DSF was performed in a 96-well plate using an Mx3005p RT-PCR machine (Stratagene) with excitation and emission filters of 492 and 610 nm, respectively. Each 20 µL reaction consisted of 2 µL protein (final concentration of 2 µM) and (if applicable) 2 µL ligand at various concentrations in DSF buffer (150 mM KCl, 10 mM HEPES pH 7.5) to which 2 µL SYPROorange, diluted 500-fold in DSF buffer from the manufacturers stock (Invitrogen), was added. Fluorescence intensities were measured at each 1°C temperature increase from 25 to 96°C with a ramp rate of 3°C/min.

Crystallization and structure determination

For the glyoxylate-bound structure, crystals were grown by vapour diffusion at 20°C in a sitting drop consisting of 50 nL of protein (12 mg/ml) and 100 nL well solution, equilibrated against well solution containing 30% PEG 1000, 0.1 M Malate-MES-Tris pH 7.0. For the glycolate-bound structure, crystals were grown by vapour diffusion at 4°C in sitting drops consisting 100 nL protein (13.7 mg/mL) and 50 nL well solution, equilibrated against well solution containing either 20% PEG3350, 0.1 M bis-tris-propane pH 7.5, 10% ethylene glycol, 0.2 M sodium nitrate. Crystals for the CCPST-bound structure were grown from protein pre-incubated with 2 mM CCPST, equilibrated against well solution containing 30% PEG1000, sodium malonate-imidazole-boric acid pH 8.0 (6GMC). Crystal was cryo-protected with 20-25% ethylene glycol before flash-cooling in liquid nitrogen.

The initial structure of hHAO1 (PDB 2NZZ) was solved by molecular replacement with the program PHASER (11), using published structure of spinach glycolate oxidase (PDB 1GOX) as search model (54.6% sequence identity). Bound FMN and glyoxylate in the active site were identified by difference Fourier method and manually placed into the electron density using Coot (12). Iterative cycles of refinement with SHELXL (13) followed by manual model building using Coot were performed. All subsequent hHAO1 structures were

solved by molecular replacement with PHASER using 2NZL as the search model, followed by iterative cycles of REFMAC5 (14) including TLS refinement, and manual model building in Coot.

Crystallography-based fragment screening

To launch fragment soaking campaign, crystals were grown by vapour diffusion at 4°C in sitting drops of 13.7 mg/mL protein equilibrated against well solution containing 25-35% PEG1000, sodium malonate-imidazole-boric acid pH 8.0. Approximately 50 crystals of suitable size were identified per 96-well crystallisation plate, and a total of 10 plates generated sufficient crystals for the entire fragment campaign.

For soaking, 50 nL of each fragment compound (final concentration of 125 mM) was added to a crystallization drop using an ECHO acoustic liquid handler dispenser at the Diamond light source XChem facility. Crystals were soaked for two hours with fragments from the Diamond-SGC Poised Library before being harvested using XChem SHIFTER technology, cryo-cooled in liquid nitrogen, and data sets collected at the beamline I04-1 in “automated unattended” mode. The XChemXplorer pipeline (15) was used for structure solution with parallel molecular replacement using DIMPLE (template 2NZL) (16), followed by map averaging and statistical modelling to identify weak electron densities generated from low occupancy fragments using Pandda software (17). Coordinates and structure factors for all data sets with bound fragments are deposited in the RCSB Protein Data Bank. The crystal structures displaying conformational changes in loop 4 (fragment 1, 5QIB; fragment 2, 5QIH; and fragment 5, 5QIC) were deposited containing coordinates for both the fragment-bound and ground states for the loop.

References

1. Williams, E. L., Acquaviva, C., Amoroso, A., Chevalier, F., Coulter-Mackie, M., Monico, C. G., Giachino, D., Owen, T., Robbiano, A., Salido, E., Waterham, H., and Rumsby, G. (2009) [Primary hyperoxaluria type 1: update and additional mutation analysis of the AGXT gene](#). *Hum Mutat* **30**, 910-917
2. Danpure, C. J. (2005) [Primary hyperoxaluria: from gene defects to designer drugs?](#) *Nephrol Dial Transplant* **20**, 1525-1529
3. Martin-Higueras, C., Torres, A., and Salido, E. (2017) [Molecular therapy of primary hyperoxaluria](#). *J Inherit Metab Dis* **40**, 481-489
4. Williams, E., Cregeen, D., and Rumsby, G. (2000) [Identification and expression of a cDNA for human glycolate oxidase](#). *Biochim Biophys Acta* **1493**, 246-248
5. Frishberg, Y., Zeharia, A., Lyakhovetsky, R., Bargal, R., and Belostotsky, R. (2014) [Mutations in HAO1 encoding glycolate oxidase cause isolated glycolic aciduria](#). *J Med Genet* **51**, 526-529
6. Li, X., Knight, J., Fargue, S., Buchalski, B., Guan, Z., Inscho, E. W., Liebow, A., Fitzgerald, K., Querbes, W., Todd Lowther, W., and Holmes, R. P. (2016) [Metabolism of \(13\)C5-hydroxyproline in mouse models of Primary Hyperoxaluria and its inhibition by RNAi therapeutics targeting liver glycolate oxidase and hydroxyproline dehydrogenase](#). *Biochim Biophys Acta* **1862**, 233-239
7. Dutta, C., Avitahl-Curtis, N., Pursell, N., Larsson Cohen, M., Holmes, B., Diwanji, R., Zhou, W., Apponi, L., Koser, M., Ying, B., Chen, D., Shui, X., Saxena, U., Cyr, W. A., Shah, A., Nazef, N., Wang, W., Abrams, M., Dudek, H., Salido, E., Brown, B. D., and Lai, C. (2016) [Inhibition of Glycolate Oxidase With Dicer-substrate siRNA Reduces Calcium Oxalate Deposition in a Mouse Model of Primary Hyperoxaluria Type 1](#). *Mol Ther* **24**, 770-778
8. Liebow, A., Li, X., Racie, T., Hettlinger, J., Bettencourt, B. R., Najafian, N., Haslett, P., Fitzgerald, K., Holmes, R. P., Erbe, D., Querbes, W., and Knight, J. (2017) [An Investigational RNAi Therapeutic Targeting Glycolate Oxidase Reduces Oxalate Production in Models of Primary Hyperoxaluria](#). *J Am Soc Nephrol* **28**, 494-503
9. Bradley, A. R., Echalié, A., Fairhead, M., Strain-Damerell, C., Brennan, P., Bullock, A. N., Burgess-Brown, N. A., Carpenter, E. P., Gileadi, O., Marsden, B. D., Lee, W. H., Yue, W., Bountra, C., and von Delft, F. (2017) [The SGC beyond structural genomics: redefining the role of 3D structures by coupling genomic stratification with fragment-based discovery](#). *Essays Biochem* **61**, 495-503

10. Summitt, C. B., Johnson, L. C., Jonsson, T. J., Parsonage, D., Holmes, R. P., and Lowther, W. T. (2015) [Proline dehydrogenase 2 \(PRODH2\) is a hydroxyproline dehydrogenase \(HYPDH\) and molecular target for treating primary hyperoxaluria](#). *Biochem J* **466**, 273-281
11. McCoy, A. J., Grosse-Kunstleve, R. W., Storoni, L. C., and Read, R. J. (2005) [Likelihood-enhanced fast translation functions](#). *Acta Crystallogr. D Biol. Crystallogr.* **61**, 458-464
12. Emsley, P., and Cowtan, K. (2004) [Coot: model-building tools for molecular graphics](#). *Acta Crystallogr. D Biol. Crystallogr.* **60**, 2126-2132
13. Sheldrick, G. M. (2008) [A short history of SHELX](#). *Acta Crystallogr. A* **64**, 112-122
14. Murshudov, G. N., Vagin, A. A., and Dodson, E. J. (1997) [Refinement of macromolecular structures by the maximum-likelihood method](#). *Acta Crystallogr. D Biol. Crystallogr.* **53**, 240-255
15. Krojer, T., Talon, R., Pearce, N., Collins, P., Douangamath, A., Brandao-Neto, J., Dias, A., Marsden, B., and von Delft, F. (2017) [The XChemExplorer graphical workflow tool for routine or large-scale protein-ligand structure determination](#). *Acta Crystallogr D Struct Biol* **73**, 267-278
16. Winn, M. D., Ballard, C. C., Cowtan, K. D., Dodson, E. J., Emsley, P., Evans, P. R., Keegan, R. M., Krissinel, E. B., Leslie, A. G., McCoy, A., McNicholas, S. J., Murshudov, G. N., Pannu, N. S., Potterton, E. A., Powell, H. R., Read, R. J., Vagin, A., and Wilson, K. S. (2011) [Overview of the CCP4 suite and current developments](#). *Acta Crystallogr D Biol Crystallogr* **67**, 235-242
17. Pearce, N. M., Krojer, T., Bradley, A. R., Collins, P., Nowak, R. P., Talon, R., Marsden, B. D., Kelm, S., Shi, J., Deane, C. M., and von Delft, F. (2017) [A multi-crystal method for extracting obscured crystallographic states from conventionally uninterpretable electron density](#). *Nat Commun* **8**, 15123

We respectfully request that this document is cited using the DOI value as given above if the content is used in your work.